ChemComm

Surface-Enhanced Raman Spectroscopy (SERS): A powerful technique to study the SEI layer in batteries

Journal:	*ChemComm*
Manuscript ID	CC-COM-12-2020-008001
Article Type:	Communication

COMMUNICATION

Surface-Enhanced Raman Spectroscopy (SERS): A powerful technique to study the SEI layer in batteries

M. J. Piernas-Muñoz,[a,b,*] A. Tornheim,[a] S. Trask,[a] Z. Zhang[a] and I. Bloom[a,*]

Received 00th January 20xx,
Accepted 00th January 20xx

DOI: 10.1039/x0xx00000x

The solid electrolyte interphase (SEI) layer on a silicon anode is investigated by SERS. Gold electrodeposition on a silicon electrode is confirmed by SEM, and Raman enhancement is proved, allowing determination of the partial composition of its SEI. For the first time, organophosphate-derivatives seem to be detected by Raman.

Silicon anodes are being partially implemented in electric vehicles to increase the energy density of current Li-ion batteries (LIB), which are dominated by graphitic anodes. Although the capacity of silicon (3579 $mAhg^{-1}$)[1] is almost ten times higher than that of graphite (372 $mAhg^{-1}$)[2], silicon suffers from rapid capacity fading because of the large volume expansion of ca. 300% it undergoes during lithiation[3] and the subsequent shrinkage experienced during delithiation, which leads to particle cracking and pulverization, resulting in electrical isolation of the active material.[4,5]

Also, as a result of this expansion/contraction, the SEI layer formed on the surface of silicon is repeatedly formed/fractured during the lithiation/delithiation processes.[6,7] Since the formation of a robust SEI layer is key for the stability and durability of battery operation,[8,9] the investigation of its composition is crucial for understanding how this technology works, i.e., which components are beneficial and which are detrimental in the passivation of the anode. Unfortunately, the nature of the silicon SEI is yet not well-defined, as its morphology, thickness, and composition depend on the electrolyte, additives and the electrode binder used.[10]

SERS is a powerful technique that involves the presence of noble metal, such as gold or silver, nanoparticles (NPs) in the proximity of part of a sample to be studied.[11] When these NPs are excited by visible light, they absorb energy that enables collective electron oscillations inside the NPs that generate a wave or localized surface plasmon resonance (LSPR). In turn, this creates a local field around the NPs that polarizes the molecules located near them and Raman scattering occurs.[12] The interaction of the Raman field with the metallic NPs generates a new field, the intensity of which depends on the 4th power to the initial field, leading to the SERS or Raman enhancement.[11] The local field can be further enhanced by the so-called lightning rod effect, if rough metallic NPs surfaces are used.[13] In summary, the intensity of the Raman scattering by a species of interest, silicon in our case, can be enhanced by the presence of certain nanostructured metals.

The first SERS phenomenon was reported by Fleischman *et al*. in 1974, who detected the Raman spectrum of a pyridine monolayer using rough silver electrodes.[14] Although SERS has been widely used ever since in several applications such as surface, biological and analytical sciences,[15] the examples published involving SERS in the battery field are but a handful. Some of the studies were performed in Li-air batteries by Peter Bruce *et al*. in 2011 and 2012, using roughened Au electrodes, with the objective of proving/refuting the formation of Li_2O_2 when using organic carbonate,[16] acetonitrile[17] or dimethyl sulfoxide[18] electrolytes. Liu *et al.* also explored the reaction process occurring on conductive substrates, such as a gold film or graphene Li-air cathodes.[19] In fact, most research has been dedicated to investigating the cathode side of Li-air or LIB. For instance, Hy and co-workers demonstrated the formation of Li_2O on Li-rich cathodes, $LiNi_{0.5}Mn_{0.5}O_2$ and $Li_{1.2}Ni_{0.2}Mn_{0.6}O_2$.[20] Tornheim *et al.* enhanced the Raman signal of pristine Ni-rich $LiNi_{0.5}Co_{0.2}Mn_{0.3}O_2$ resulting in a 70-fold signal increase of the normally weak signal associated with Ni-rich compounds.[21] Li *et al.* evaluated changes in the cathode electrolyte interphase (CEI) of $LiNi_xMn_yCo_{1-x-y}O_2$ (NCM811 and NCM111).[22] Only few articles from groups led by Passerini, Winter and Mao, and Hardwick proposed to examine the products formed on Li metal anode surfaces with the aim of identifying the SEI products.[2223, 24, 25, 26] In this context, Hy *et al.* reported the study of graphite[19] and SiO_2 anodes,[27] the latter in ethylene carbonate:diethyl carbonate (EC:DEC) electrolyte with and without vinylene

[a] *Chemical Sciences and Engineering Division, Argonne National Laboratory, Lemont, Illinois, 60349, U.S.A.*
[b] *Currently at Department of Inorganic Chemistry, University of Murcia and Institute for Bio-Health Research, Murcia, 30071, Spain.*
** corresponding authors: mjpiernas@um.es; ira.bloom@anl.gov*

Electronic Supplementary Information (ESI) available. See DOI: 10.1039/x0xx00000x

carbonate (VC). One of the latest works, conducted by Nanda and collaborators, focused on determining electrolyte solvation at the solid/liquid interface.[28]

In this communication, we deposit Au NPs on a silicon electrode and employ SERS to examine the SEI layer formed when this material is electrochemically cycled in a Li-ion battery. The noble metal commonly used for SERS is gold (Au) due to its higher stability and ease of synthesis as compared to other metal substrates. For the purpose of this study, Au NPs were deposited on top of the silicon electrodes by electrodeposition, as illustrated in **Figure S1**, following the procedure detailed in the Supplementary Information (SI) (see *Au-NPs@silicon electrodes* section). The presence of Au was confirmed by Scanning Electron Microscopy (SEM) (**Figure 1** and **Figure S2**) and Energy Dispersive X-Ray Spectroscopy (EDS) (**Figure S3**). The homogeneity of the pristine silicon electrode observed in **Figure 1a** evolves to a more heterogeneous and rough topography (**Figure 1c**) after coating its surface with gold, where domains of non-coated (darker) and coated (lighter) areas are distinguished. This is even more obvious when a BSED (back-scattered electron detector) is used, as **Figure S2** illustrates. A closer look at the electrodes not only reveals that the porosity of the initial electrode (**Figure 1b**) is reduced after the electrodeposition (**Figure 1d** and **Figure S2b**) but also provides an estimation of the shape and particle size of the Au NPs covering the silicon, which are either spheroidal or irregular as they aggregate, and are approximately in the range of tens to hundreds of nanometers.

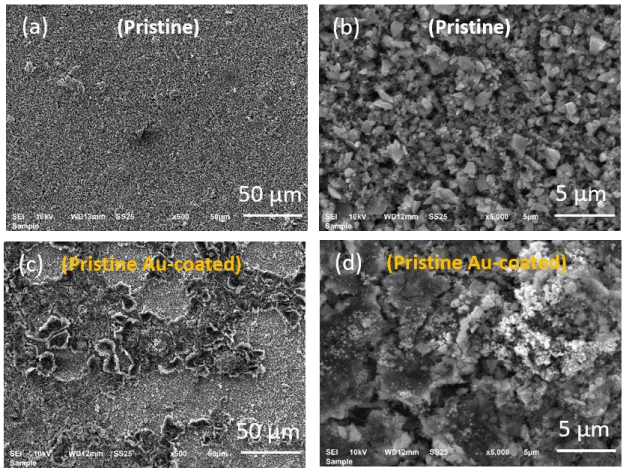

Figure 1. SEM micrographs of the pristine silicon electrode (a, b) and the Au-coated silicon electrode (c, d) at two different magnifications (x500, scale bar 50 µm; and x5000, scale bar 5 µm).

Raman analysis indicated an average Raman enhancement factor of at least 5 and a maximum enhancement factor of 8 when comparing the pristine Au-coated silicon electrodes to the pristine non-Au-coated electrodes (**Figure 2a**). The enhancement factor was calculated by normalizing the spectra to an internal $Na_4Fe(CN)_6{\cdot}10H_2O$ standard (added to the silicon samples) and averaged, while the maximum enhancement factor was obtained without averaging. Even though an enhancement factor of ca. 10 may not be appealing in principle, it is enough to allow detection and identification of several species. Although only the typical band corresponding to crystalline silicon at 520 cm^{-1} is detected in the pristine non-Au-coated silicon electrode (**Figure 2a**, black line), its transverse acoustic mode and its second and third overtones, respectively, at ca. 300, 943 and 1491 cm^{-1}, as well as the characteristic D- and G-bands of the conductive carbon at ~1342 and 1577 cm^{-1}, can be clearly observed in the Raman spectra of the Au-coated silicon electrodes (**Figure 2a**, red and gold lines). A slight shift of the Raman peak from Si is observed, from 520 to 517 cm^{-1}, in the Au-coated electrodes. The weak cyanide stretching vibrations, $\nu_{C\equiv N}$, from the $Na_4Fe(CN)_6{\cdot}10H_2O$ standard are also present in all the spectra at 2074 and 2104 cm^{-1} (see **Figure S4** for reference). The assignment of these Raman bands is based on previous studies.[29, 30, 31, 32]

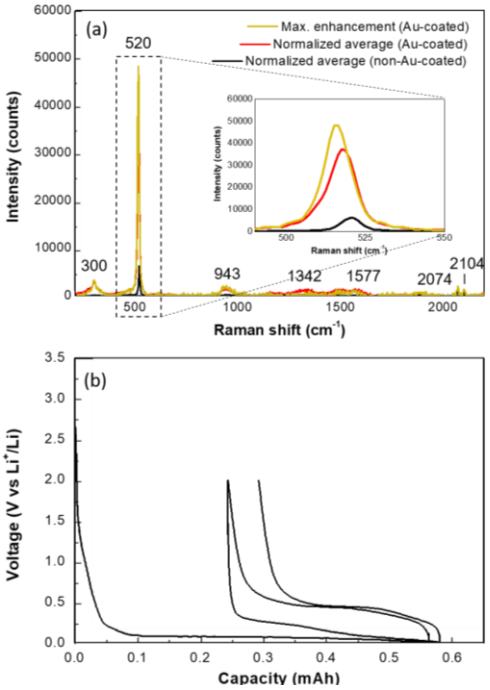

Figure 2. (a) Raman spectra of pristine silicon electrodes in black and Au-coated pristine silicon electrodes in red (average enhancement) and gold (maximum enhancement), and (b) electrochemical voltage profile of the first two cycles of silicon *vs.* Li^+/Li, cycled with Gen 2 electrolyte.

In order to form the SEI layer, the Au-coated and non-Au-coated silicon electrodes were galvanostatically cycled twice in the voltage range of 10 mV to 2 V *vs*. Li^+/Li, using the Gen 2 (1.2 M $LiPF_6$ EC/EMC (3/7)) electrolyte. The SI provides further details. Its voltage profile is plotted in **Figure 2b** and shows the typical charge voltage plateau below 100 mV and the discharge‡ plateau at ca. 0.3-0.4 V *vs*. Li^+/Li. These values agree with those previously reported in the literature for silicon,[5,6] suggesting that the presence of Au does not significantly affect the electrochemistry of silicon. The loss in reversible capacity experienced by silicon from the first cycle to the second is also noted. The cells were then disassembled in an argon-filled glove box with water and oxygen levels below 1 ppm. The silicon electrodes were extracted; carefully rinsed with anhydrous

dimethyl carbonate, allowed to dry and analyzed by SEM and Raman. **Figure 3** contrasts the differences between the cross-section images of the non-Au-coated and Au-coated pristine electrodes (a-d) with cycled electrodes (e, f). It is interesting to note that the thickness of the pristine electrode remains almost constant after the Au electrodeposition. Conversely, the cycled electrodes (**Figure 3e, f**) experience a huge volume expansion, as expected.[3] The coating layer, initially ca. 10-15 µm thick, expands to almost 50 µm. Besides, the gold appears to be homogeneously distributed (**Figure 3f**).

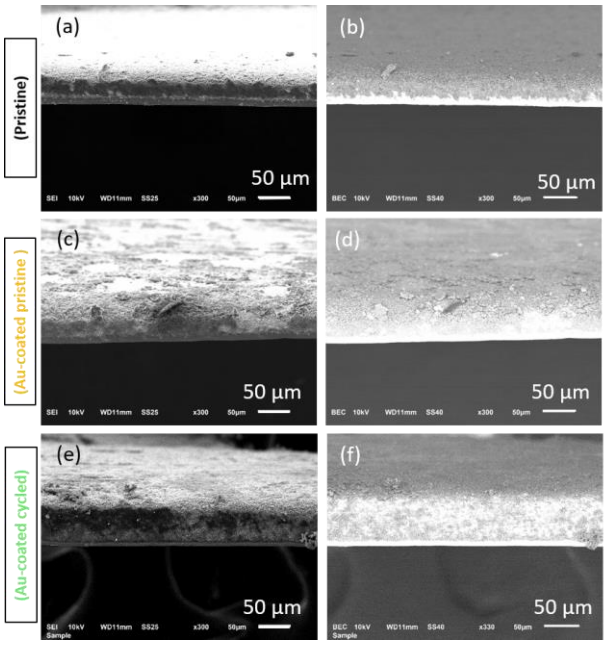

Figure 3. SEM cross-sections of the silicon pristine (a, b), Au-coated silicon pristine (c, d) and Au-coated silicon cycled electrodes (e, f). Images on the left were taken with the secondary electron detector, while those on the right were obtained with the BSED.

In contrast to the non-Au-coated cycled electrode (**Figure 4a**) where Raman bands are almost non-existent, except for one at 511 cm^{-1} indicative of nanosized silicon, the Raman enhancement in the Au-coated cycled sample is evident, as several bands can be seen (**Figure 4b**). A tentative assignment of these bands is given in **Table S1** of the SI file, and a brief discussion of these results follows. The signal at ca. 467 cm^{-1} is associated with amorphous silicon (a-Si), which is known to be formed after the first electrochemical cycle of the silicon electrode.[33] The transverse acoustic mode of silicon,[29] observed in the pristine electrode (**Figure 2a**), is still present at 298 cm^{-1} after cycling. Regarding other silicon-based species that can be identified, we also observe vibrations at 980 and 1084 cm^{-1}, that we attribute, respectively, to Si-OH[34] or the symmetric stretching of Si-O[35,36] and to O-Si-O,[37,38] typical of SiO_2 or silicates (Li_xSiO_y). The reactivity of lithium with silicon and its SiO_2 surface layer is known to lead to the formation of Li_2O and lithium silicate in the silicon SEI after the first lithiation of the material.[39] Nevertheless, it is important to note that the band at 980 cm^{-1} can also overlap with the second transverse optic (TO) mode of silicon.[31] Likewise, the band at 1084 cm^{-1} also could be due to Li_2CO_3,[24,27] one of the predominant components of the inorganic layer that forms the SEI of anodes in LIB and which has been reported as necessary to form an effective passivation[40] layer that blocks electrons but allows ion migration. In fact, this double-assignment to Li_2CO_3 and a mixture of lithium silicates has been previously proposed[38] for a band centered at 1080 cm^{-1}. Another signal ascribed to Si-O vibrations[37] or Si-CH_3[30] appears at 1280 cm^{-1}.

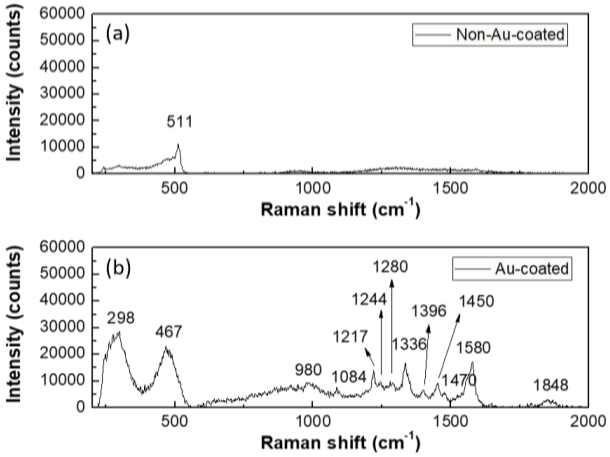

Figure 4. Raman spectra of cycled silicon electrodes, (a) non-Au-coated and (b) Au-coated.

On the other hand, as far as carbon-related species are concerned, the D- (1336 cm^{-1}) and G-bands (1580 cm^{-1})[30] of the conductive C45 carbon additive remain unaltered in the cycled material. A peak at 1217 cm^{-1}, that could correspond to C-C stretching vibrations of lithium alkyl carboxylates,[41] is distinguished as well. In addition, there are three more signals at 1244, 1396 and 1450 cm^{-1}, which may be associated with different C-H vibrational modes,[29,42] some of them suggesting the possible generation of olefinic fragments (another common component of the SEI[8]). Alternatively, the vibrations observed at approx. 1217, 1244 and 1395 cm^{-1} are also compatible with the stretching $\nu_{P=O}$ modes of organophosphorus compounds, such as $(CH_3)_2P(=O)CH_3$, $P(=O)F_3$ and PO_3^{2-}.[42] Organophosphate and derivative compounds are typical decomposition products of $LiPF_6$ salt, since $LiPF_6$ (in equilibrium with LiF/PF_5) reacts in the presence of trace water to form POF_3, which subsequently evolves to organophosphate and organic fluorophosphate-based products.[44] To the best of our knowledge, this is the first time that organophosphorus derivatives have been detected in an electrode SEI by Raman, as they generally have been found by High-Performance Liquid Chromatography-Mass Spectrometry (HPLC-MS), Gas Chromatography-Mass Spectrometry (GC-MS) or X-Ray Photoelectron Spectroscopy (XPS). Only a recent study investigating the aging of $LiPF_6$ salt by Kerr gated Raman identified POF_3 at ca. 900 cm^{-1} on the $LiPF_6$ surface, although this was due to its hydrolysis after adding water.[43] However, we did not find spectral evidence for POF_3.

Curiously, although not very intense, another signal is seen at 1848 cm^{-1}. According to the literature, it could be due to the formation of lithium acetylide, Li_2C_2,[25] which has been recently proposed as a lithium plating/deposition marker.[45]

Even though an average Raman enhancement factor of 5 was initially calculated from the pristine electrodes (**Figure 2**), the intensity of the Au-coated spectra for the cycled sample (**Figure 4**) makes us think that the enhancement may be several-fold higher. A plausible explanation is that, as a result of the electrode and coating heterogeneity, as well as the porous nature thereof, the enhancement will probably vary from one region to another. Additionally, the electrochemical cycling may have an effect on the observed enhancement. Li and Au are known to alloy and could maximize the SERS effect.[46] On the other hand, besides the LSPR, contributions from the lightning rod effect of rough surfaces may also be present.[13]

In summary, a silicon electrode was gold-coated by electrodeposition to study its SEI. SEM images have confirmed a non-uniform gold layer on top of silicon, and later Raman analysis showed that the average enhancement factor was ~5. After electrochemically cycling the Au-coated silicon electrode, several more bands were detected by Raman as compared to the non-Au-coated sample. SERS allowed the partial determination of SEI components, such as Li_xSiO_y, Li_2CO_3, alkylcarbonates and olefins or organophosphate-based (P=O) compounds. Since this tool has been used with different materials and technologies within the Li-ion battery family, we firmly believe that SERS could serve as a complementary technique in other battery systems, such as Na-, K-, Mg- or Al-ion batteries, and could help in understanding the nature of the SEI, which is key for long and safe battery operation.

We gratefully acknowledge support from Brian Cunningham at the U. S. Department of Energy (DOE), Vehicle Technologies Office. Argonne National Laboratory´s work was supported by the U.S. DOE Vehicle Technologies Office under contract number DE-AC02-06CH11357.

There are no conflicts of interest to declare.

Notes and references

‡ It is important to note here that we are using a full-cell criterion. Hence, when talking about charging, we refer to full-cell charge, i.e., silicon lithiation. Conversely, discharging relates to silicon delithiation.

1 M. N. Obrovac and L. Christensen, *Electrochem. Solid-State Lett.*, 2004, **7**, A93-A96.
2 J. M. Tarascon, M. Armand, *Nature*, 2001, **414**, 359-367.
3 M. N. Obrovac, J. L. Krause, *J. Electrochem. Soc.*, 2007, **154**, A103-A108.
4 M. T. McDowell, S. W. Lee, W. D. Nix, Y. Cui, *Adv. Mater.*, 2013, **25**, 4966-4985.
5 W-J. Zhang, *J. Power Sources*, 2011, **196**, 13-24.
6 J. Wook Choi, D. Aurbach, *Nat. Rev. Mater.,* 2016, **1**, 16013.
7 X. Su, Q. Wu, J. Li, X. Xiao, A. Lott, W. Lu, B. W. Sheldon, J. Wu, *Adv. Energy Mater*., 2014, **4**, 1300882.
8 E. Peled and S. Menkin, *J. Echem. Soc.*, 2017, **164** (7), A1703-A1719.
9 B. Philippe, R. Dedryvère, M. Gorgoi, H. Rensmo, D. Gonbeau, K. Edström, *Chem. Mater*., 2013, **25**, 394-404.
10 P. Verma, P. Maire, P. Novák, *Echim. Acta*, 2010, **55**, 6332-6341.
11 P. L. Stiles, J. A Dieringer, N. C. Shah, R. P. Van Duyne, *Annu. Rev. Anal. Chem*., 2008, **1**, 601-626.
12 N. Guillot, M. Lamy de la Chapelle, *J. Quant. Spectrosc. Ra.*, 2012, **113**, 2321-2333.
13 J. Gersten, A. Nitzan, *J. Chem. Phys*., 1980, **73**(7), 3023.
14 M. Fleischmann, P. J. Hendra, A. J. McQuillan, *Chem. Phys. Lett*., 1974, **26**, 163-166.
15 Q. Zhou, G. Meng, P. Zheng, S. Cushing, N. Qu, Q. Huang, C. Zhu, Z. Zhang, Z. Wang, *Sci. Rep*., 2015, **5**, 12865.
16 S. A. Freunberger, Y. Chen, Z. Peng, J. M. Griffin, L. J. Hardwick, F. Bardé, P. Novák, P. G. Bruce, *J. Am. Chem. Soc*., 2011, **133**, 8040-8047.
17 Z. Peng, S. A. Freunberger, L. J. Hardwick, Y. Chen, V. Giordani, F. Bardé, P. Novák, D. Graham, J-M. Tarascon, P. G. Bruce, Angew, *Chem. Int. Ed.*, 2011, **50**, 6351-6355.
18 Z. Peng, S. A. Freunberger, Y. Chen, P. G. Bruce, *Science*, 2012, **337**, 563-566.
19 K. Liu, Z. Yu, S. Zhang, F. Zou, Y. Zhu., *RSC Adv.*, 2016, **6**, 102272.
20 S. Hy, F. Felix, J. Rick, W-N. Su, B. J. Hwang, *J. Am. Chem. Soc*., 2014, **136**, 999-1007.
21 A. Tornheim, V. A. Maroni, M. He, D. J. Gosztola, Z. Zhang, *J. Electrochem. Soc.*, 2017, **164** (13), A3000-A3005.
22 C-Y. Li, Y. Yu, C. Wang, Y. Zhang, S-Y. Zheng, J-F. Li, F. Maglia, R. Jung, Z-Q. Tian, Y. Shao-Horn, *J. Phys. Chem. C*, 2020, **124**, 4021-4031.
23 R. Schmitz, R. A. Müller, R. W. Schmitz, C. Schreiner, M. Kunze, A. Lex-Balducci, S. Passerini, M. Winter, *J. Power Sources*, 2013, **233**, 110.
24 S. Tang, Y. Gu, J. Yi, Z. Zeng, S-Y. Ding, J-W. Yan, D-Y. Wu, B. Ren, Z-Q. Tian, B-W. Mao, *J. Raman Spectrosc*., 2016, **47**, 1017-1023.
25 T. A. Galloway, L. Cabo-Fernández, I. M. Aldous, F. Braga, L. Hardwick, *Faraday Discuss*., 2017, **205**, 469.
26 A. J. Cowan, L. J. Hardick, *Annu. Rev. Anal. Chem*. 2019, **12**, 323-346.
27 S. Hy, F. Felix, Y-H. Chen, J-y. Liu, J. Rick, B-J, Hwang, *J. Power Sources*, 2014, **256,** 324-328.
28 G. Yang, I. N. Ivanov, R. E. Ruther, R. L. Sacci, V. Subjakova, D. T. Hallinan, J. Nanda, *ACS Nano*, 2018, **12**, 10159-10170.
29 B. Han, M. J. Piernas-Muñoz, F. Dogan, J. Kubal, S. E. Trask, I. D. Bloom, J. T. Vaughey, B. Key. *J. Electrochem. Soc*., 2019, **166** (12), A2396.
30 M. J. Piernas-Muñoz, S. E. Trask, A. R. Dunlop, E. Lee, I. Bloom, *J. Power Sources,* 2019, **441**, 227080.
31 G. Yang, X. Li, Y. Cheng, M. Wang, D. Ma, A. Sokolov, S. Kalinin, G. Veith, J. Nanda, DOI: 10.21203/rs.3.rs-38466/v1
32 P. A. Temple, C. E. Hathaway, *Phys. Rev. B*, 1973, **7**, 3685.
33 K. Ogata, E. Salager, C. J. Kerr, A. E. Fraser, C. Ducati, A. J. Morris, S. Hoffmann, C. P. Grey, *Nature Commun*., 2014, **5**, 3217.
34 A. K. Yadav, P. Singh, *RSC. Adv*., 2015, **5**, 67583-67609.
35 L. Salazar Hoyos, B. Faroldi, L. Corgnaglia, *J. Alloys Compd*., 2019, **778**, 699-711.
36 M. Choi, J-C. Kim, D-W. Kim, *Sci. Rep*., 2018, **8**, 960.
37 M. Yu, D. P. Abraham, Y. Chen, A. Bose, B. L. Lucht, *J. Phys. Chem. C,* 2013, **117**, 13403-14312.
38 K. Richter, T. Waldmann, M. Kasper, C. Pfeifer, M. Memm, P. Axmann, M. Wohlfahrt-Mehrens. *J. Phys. Chem. C,* 2019, **123**, 18795-18803.
39 B. Phylippe, R. Dedryvère, M. Gorgoi, H. Rensmo, D. Gonbeau, K. Edström, *Chem. Mater.*, 2013, **25**, 394-404.
40 K. Guo, R. Kumar, X. Xiao, B. W. Sheldon, H. Gao, *Nano Energy*, 2020, **68**, 104257.
41 S. Attralarasan, S. E. Arasi, S. Prathap, T. Gunaseelan, J. Madhavan, *IJSRST*, 2018, **4**(2), 1599-1603.
42 D. Lien-Vien, N. B. Colthup, W. G. Fateley, J. G. Grasselli. Infrared and Raman Characteristic frequencies of Organic Molecules; Academic Press: San Diego, 1991. Pages 74-82 (C-H), pages 266 (P=O).
43 L. Cabo-Fernández, A. R. Neale, F. Braga, I. V. Sazanovich, R. Kostecki, L. J. Hardwick, *Phys. Chem. Chem. Phys*. 2019, **21**, 23833.
44 S. Nowak, M. Winter, *Molecules,* 2017, **22**, 403-424.
45 M-T. Fonseca Rodrigues, V. A. Maroni, D. J. Gosztola, K. P. C. Yao, K. Kalaga, A. Shkrob, D. P. Abraham., *Appl. Energy Mater*., 2019, **2**, 873.
46 P. Bach, I. Valencia-Jaime, U. Rütt, O. Gutowski, A. H. Romeo, F. U. Renner, *Chem. Mater*. 2016, **28**(9), 2941-2948.

